The Astrophysical Journal, 740:85 (9pp), 2011 October 20 doi:10.1088/0004-637X/740/2/85

TRANSIENT SUPERSTRONG CORONAL LINES AND BROAD BUMPS IN THE GALAXY SDSS J074820.67+471214.3

Ting-Gui Wang[1,2], Hong-Yan Zhou[1,2,3], Li-Fan Wang[4], Hong-Lin Lu[1,5], and Dawei Xu[6]
[1] Key Laboratory for Research in Galaxies and Cosmology, Chinese Academy of Sciences, The University of Sciences and Technology of China (USTC), Hefei, Anhui 230026, China; twang@ustc.edu.cn
[2] Center for Astrophysics, USTC, Hefei, Anhui 230026, China
[3] Polar Research Institute of China, 451 Jinqiao Road, Pudong, Shanghai 200136, China
[4] Department of Physics, Texas A&M University, College Station, TX 77843, USA
[5] Physics Experiment Teaching Center, USTC, Hefei, Anhui 230026, China
[6] National Astronomical Observatories, Chinese Academy of Sciences, 20A Datun Road, Chaoyang District, Beijing 100012, China
Received 2010 July 2; accepted 2011 July 22; published 2011 October 3

ABSTRACT

Variable superstrong coronal emission lines were observed in the spectrum of one galaxy, SDSS J095209.56+214313.3, and their enigmatic origin remains controversial. In this paper, we report the detection of variable broad emission bumps reminiscent of a supernova (SN) II-Plateau spectra taken a few days after the shock breakout in a second galaxy with variable superstrong coronal lines, SDSS J074820.67+471214.3. The coronal line spectrum shows unprecedentedly high ionization with superstrong [Fe x]λ6376, [Fe xi]λ7894, [Fe xiv]λ5304, [S xii]λ7612, and [Ar xiv]λ4414, but without detectable optical [Fe vii] line emission. The coronal line luminosities are similar to those observed in bright Seyfert galaxies and 20 times more luminous than those reported in the hottest Type IIn SN 2005ip inferred from its strong coronal lines. The coronal lines ($\sigma \sim 120$–240 km s^{-1}) are much broader than the narrow emission lines ($\sigma \sim 40$ km s^{-1}) from the star-forming regions in the galaxy, but are nearly at the same systematic redshift. We also detected a variable non-stellar continuum emission from its Sloan Digital Sky Survey spectroscopy and *Galaxy Evolution Explorer* photometry. In the follow-up spectra taken 4–5 years later, the coronal lines, SN-like feature, and non-stellar continuum disappeared, while the [O iii]λ5007 intensity increased by a factor of about 10. Our analysis suggests that the coronal line region should be at least 10 light days in size and should be powered either by a steady ionizing source with a soft X-ray luminosity of at least a few 10^{42} erg s^{-1} or by a very luminous soft X-ray outburst. These findings can be more naturally explained by a star tidally disrupted by the central black hole than by an SN explosion. The similarity of the coronal line variability trend observed in the two galaxies suggests that the two transient events have the same origin, with SDSS J074820.67+471214.3 being caught at an earlier stage by the spectroscopic observation.

Key words: galaxies: nuclei – line: formation – supernovae: general

Online-only material: color figures

1. INTRODUCTION

Superstrong coronal lines have been detected in two galaxies spectroscopically observed in the Sloan Digital Sky Survey (SDSS; York et al. 2000), SDSS J095209.56+214313.3 (hereafter SDSS J0952+2143; Komossa et al. 2008) and SDSS J124134.25+442639.2 (Gelbord et al. 2009). Follow-up observations of SDSS J0952+2143 showed that high-ionization coronal lines were fading on timescales of years since their discovery (Komossa et al. 2008, 2009).[7] Two physical processes were proposed for the transient coronal lines: (1) an episodic accretion onto a supermassive black hole (SMBH) following the tidal disruption of a star in the vicinity of the central black hole and (2) a peculiar-type supernova (SN) with strong coronal lines, such as the recently discovered SN2005ip (Smith et al. 2009). The former case provides a way to conduct a systematic search for the tidal disruption events through optical spectroscopic surveys, and thus can be used to constrain the stellar distribution and dynamics in the vicinity of SMBHs, as well as the circumnuclear environment. The latter case is also interesting in that, though coronal line emission in SNe is fairly well understood on the basis of current models, none of these models has been tested in these extreme cases.

Narrow coronal lines up to [Fe vii]λ6087, [Fe x]λ6376, [Fe xi]λ7894, and [Fe xiv]λ5304 were observed in the late phase of a few SNe (e.g., Gröningsson et al. 2006; Smith et al. 2009). SN2005ip is the only SN where coronal lines, together with recombination lines, were also detected in its early phase, probably a few weeks after the explosion. The coronal lines are thought to arise from the interaction between the SN and circumstellar material (CSM). The X-rays from the radiative shock ionize CSM and give rise to emission lines of a wide range of ionization states, including coronal lines. It is unclear whether superstrong coronal emitters (SSCLEs), in which coronal lines are a factor of several tens to hundreds more luminous than SN2005ip, can still be understood within this context.

Strong variable narrow coronal lines have been detected in the galactic nucleus with soft X-ray flares (Komossa & Bade 1999). The X-ray flares are thought of as a signature of stellar disruption by SMBH (e.g., Rees 1988; Bade et al. 1996; Komossa et al. 2004; Halpern et al. 2004). Thus, it is natural to associate SSCLE with the tidal disruption process. As the tidal debris settles, it forms an accretion disk around the black hole. The strong UV and X-ray radiation from the accretion disk illuminates the outer debris as well as the interstellar medium further out, giving

[7] We obtained two-epoch follow-up spectroscopic observations of SDSS J124134.25+442639.2 using the MMT 6.5 m telescope on 2008 February 11 and March 30, and found that it shows a similar variability trend as SDSS J0952+2143 (H. Y. Zhou et al. 2012, in preparation).

rise to broad and narrow high-ionization emission lines (e.g., Komossa & Bade 1999).

To distinguish between the two scenarios, it is important to find spectroscopic signatures of either an SN or a tidal disruption flare. Traditionally, core-collapse SNe have been divided into different subtypes according to their spectral signature and/or the shape of their light curve (see Filippenko 1997 for a review). The different spectral signatures arise because a different stellar evolution track of an SN progenitor leads to a different stellar radius, atmospheric chemical composition, and core mass. Most massive stars will lose their entire hydrogen and even helium envelope in the Wolf–Rayet star stage, resulting in a Type Ib or Ic SN; less massive stars will retain a hydrogen shell at the end of their evolution stage, ending with a Type II SN. A Type II SN will be further divided into Type II-L and Type II-P, depending on the lack or presence of a plateau in the light curve, which may be connected to the thickness of a hydrogen shell. Stars with a mass just above 8–10 $M_{\odot}$ will have a thick hydrogen shell at the end of a red supergiant (RSG), and explode as a Type II-P SN with a plateau in the light curve.

In this paper, we report the detection of variable broad bumps reminiscent of a young SN II-P in the spectrum of the galaxy SDSS J074820.67+471214.3 (SDSS J0748+4712 for short)—an SSCLE at a redshift of $z = 0.0616$, which was identified during a systematic search of coronal line emitters in the SDSS spectroscopic sample of galaxies. The paper is organized as follows. We present the observations, data analysis, and results in Section 2. The implications of the emission line region and ionizing continuum are discussed in Section 3. We discuss several models of SSCLEs in Section 4. Throughout this paper, we assume a Λ-dominated cosmology with $H_0 = 72$ km s^{-1} Mpc^{-1}, $\Omega_{\Lambda} = 0.7$, and $\Omega_M = 0.3$.

2. OBSERVATION AND DATA ANALYSIS

2.1. Observation, Photometric, and Spectral Data

SDSS J0748+4712 was observed by SDSS in the imaging mode on 2003 October 23. A disk galaxy was seen in this position. An SDSS spectrum centered on the nucleus was taken on 2004 February 20, about 4 months after the imaging. The galaxy was detected in the *Galaxy Evolution Explorer* (*GALEX*) survey on 2004 March 10, 20 days after the spectroscopic observation, and reobserved by *GALEX* on 2010 January 9 in NUV. Four low-resolution ($R \sim 600$) optical spectra were taken with the OMR Cassegrain spectrograph mounted on the 2.16 m telescope at the Xinglong Station of the National Astronomical Observatory of China, one on 2008 December 25, and three on 2009 March 25 with 1 hr exposure each. The spectra taken on the same night were combined. The slit was centered at the galactic nucleus with a width of 2.″0 to match the seeing disk. The galaxy was detected in the Two Micron All Sky Survey (2MASS) on 1999 February 20. The 2MASS point source catalog quoted magnitudes of $J = 16.065 \pm 0.089$, $H = 15.676 \pm 0.132$, and $K = 15.013 \pm 0.134$, with a notation of association on the extended source. Thus, these near-infrared magnitudes can only be considered as upper limits. All of the data were corrected for the Galactic extinction of $E(B - V) = 0.04$ (Schlegel et al. 1998) before further analysis.

We examined the SDSS spectrum and found three broad bumps and numerous narrow high-ionization coronal lines, including [Fe XIV]λ5304, [Fe XI]λ7894, [Fe X]λ6376, [S XII]λ7612, and [Ar XIV]λ4414, along with other lines commonly seen in an emission line galaxy, Hα, Hβ, [N II]λλ6548, 6583, [S II]λλ6716, 6732, [O III]λ5007, [O II]λ3727 (Figure 1). The broad bumps peak around 4050, 4600, and 6560 Å with widths of several hundred angstroms. These bumps do not correspond to any emission lines in an active galactic nucleus, but similar bumps are seen in the spectra of some SNe. In the figure, we overlay the spectra of Type II-P supernova SN1999gi on the day of discovery (day 1; Leonard et al. 2002), which is believed to correspond to only a few days after the shock breakout, and another Type IIP SN 2006bp, also a few days after the shock breakout (Quimby et al. 2007). It is evident that the bumps look similar to SN1999gi and SN2006bp, although their strengths are much larger. The broad bumps and coronal lines disappeared in Xinglong's spectra taken four and five years later, indicating these features are not persistent, while [O III]λ4959, 5007 brightened remarkably (Figure 2). The similarities of the broad bumps between SDSS J0748+4712 and SNe, including the centroids, profiles, and transient nature, lead us to connect both the bumps and coronal lines to an SN-like flare.

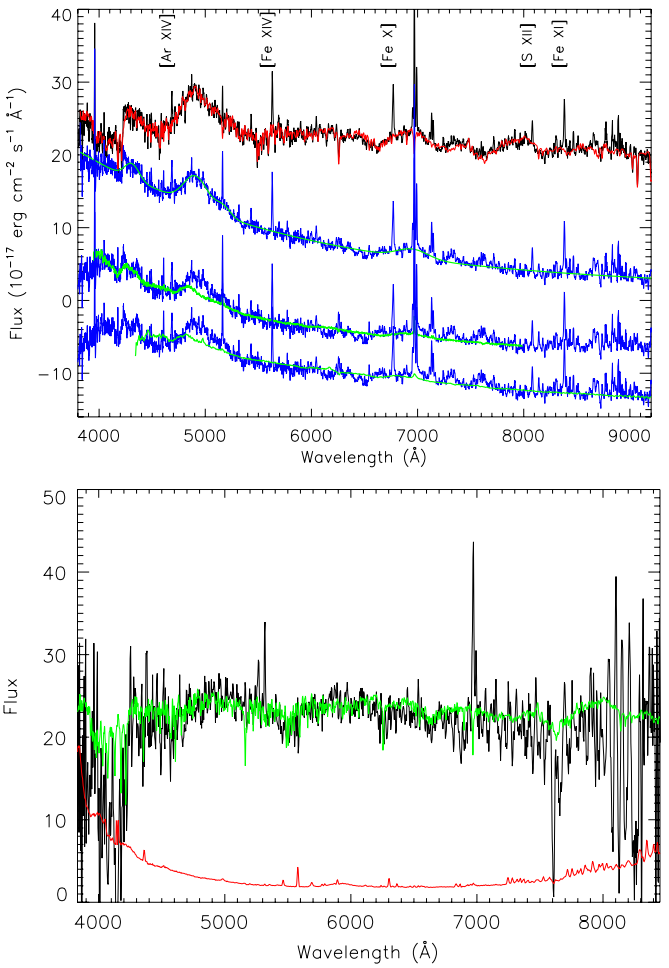

Figure 1. Upper panel: SDSS optical spectrum (in black) of SDSS J0748+4712 and the best fit (in red, see the text for details). The starlight-subtracted spectrum is plotted in blue, overlaid with different template fits (in green; models from top to bottom are blackbody+Gaussian, SN1999gi on day 1, SN 2006bp on day 1, and is shifted vertically for clarity). Coronal lines are marked. Lower panel: Xinglong spectrum of SDSS J0748+4712 overlaid with the starlight model fitted from the SDSS spectrum. The wiggle in the red part of the spectrum is due to CCD fringes. Both broad emission lines and coronal lines disappear.

(A color version of this figure is available in the online journal.)

Next, we checked the spectral energy distribution (SED; Figure 3). The synthesis magnitudes of the SDSS spectrum in *g*, *r*, and *i* bands were brighter than the fiber magnitudes determined

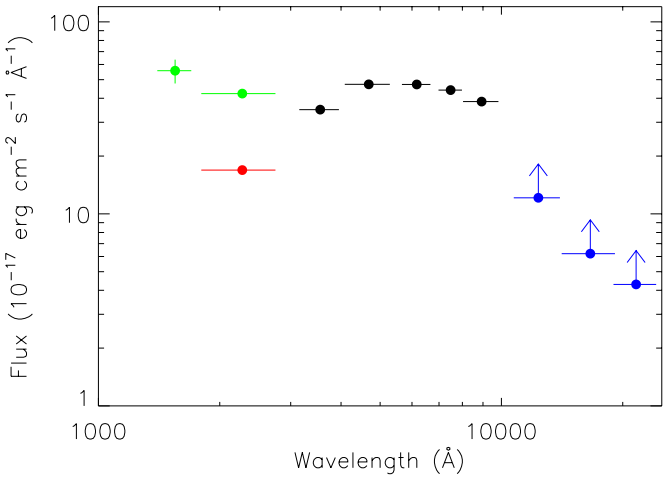

Figure 2. Broadband SED of SDSS J0748+4712. The SDSS photometric data (2003 October 23) are shown in black (model magnitudes). Near-infrared photometric data (1999 February 20) from 2MASS point source catalog, and UV photometric data on 2004 March 10 and 2010 January 9 from *GALEX* are plotted in blue, green, and red.

(A color version of this figure is available in the online journal.)

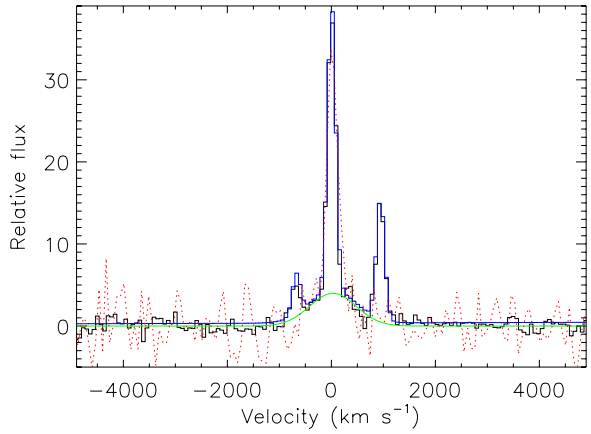

Figure 3. Hα (solid lines) profile in the SDSS spectrum. The observed Hα+[N II] is shown as black, best fit as a blue line, and the intermediate component of Hα as a green line. For comparison, the Hβ profile is overlaid as a red dashed line after it has been scaled by a factor of 2.57. Note that the continuum and very broad component have been subtracted.

(A color version of this figure is available in the online journal.)

from the SDSS imaging data by 0.51, 0.44, and 0.47 mag, respectively. The median seeing during the spectral observation was about 2.″0, similar to that used to smooth the SDSS image for a fiber magnitude estimate (Adelman-McCarthy et al. 2008); thus, fiber magnitudes properly reflect the galaxy light within the spectral fiber. However, SDSS spectra are calibrated by tying synthesis magnitudes to the point-spread function magnitudes for calibration stars; as a result, synthesis magnitudes are brighter than fiber magnitudes (Adelman-McCarthy et al. 2008). The exact difference depends on the observational conditions and the surface brightness distribution of the source. In this paper, we estimate the distribution of the difference in each band using all galaxies on the same plate of SDSS J0748+4712. These distributions are then fitted with Gaussian functions to evaluate mean deviations and their width. SDSS J0748+4712 is located far away from the main distributions in all three bands. We calculate the variations in each band by subtracting the mean difference and calculate the uncertainty by considering both the width of the distribution and the uncertainty in the synthesis magnitudes. Assuming SDSS photometric data are not affected by the SN, we estimate the magnitudes of an SN-like event to be 19.9 ± 0.24, 20.5 ± 0.09, and 19.7 ± 0.13 at g, r, and i bands. At the redshift of $z = 0.0616$, the absolute magnitudes are $M_g \approx -17.3$, $M_r \approx -16.7$, and $M_i \approx -17.5$ mag.

The 2MASS photometric fluxes are lower than SDSS fluxes, indicating that they miss part of the extended light from the galaxy. The UV fluxes on 2004 March 10 were above the simple extrapolation of optical SED, suggesting a substantial contribution from the SN-like activity. This is confirmed by the fact that the NUV magnitude on 2010 January 9 was about 0.68 mag fainter than that on 2004 March 10. Note that the NUV flux on 2010 January 9 was consistent with a natural extension of optical SED (Figure 2). Assuming that the later flux comes from starlight, the absolute NUV magnitude of the flare was $M_{\rm NUV} \approx -17.3$ mag on 2004 March 10 without considering the intrinsic reddening. The SED of the host galaxy implies that its contribution to the FUV flux on 2004 March 10 was much less than that in NUV, and FUV flux was dominated by the flare component.

2.2. Detailed Analysis of the Optical Spectrum

We first fit the SDSS spectrum with the starlight from the host galaxy and an SN template. The starlight is modeled as a combination of independent components (ICs), which are convolved with a Gaussian kernel to match the absorption line width and shifted in redshift to match the centroid of the absorption lines. The six ICs were derived by applying Ensemble Learning ICA to the simple stellar population of BC03 (refer to Lu et al. 2006 for details). A uniform extinction to the starlight is included as a free parameter.

We adopt Peter Nugent's SN templates[8] for the SN component. The templates include 439 spectra of different type SNe with several ages, including Type Ia, Type Ib, Type Ibc, Type II-L, Type II-P, and Type II-n, and peculiar Type Ia supernova, SN 1991bg and SN 1991t. Because of the similarity of SDSS J0748+4712 to the early spectra of SN 1999gi (II-P), SN 2006bp (II-P; Immler et al. 2007; Quimby et al. 2007), and SN1991N (Type Ic/b; Filippenko & Korth 1991), we also include these spectra from the SUSPECT project[9] (see Leonard et al. 2002; Quimby et al. 2007; Matheson et al. 2001 for the original spectra). The optical spectra of the last three SNe were corrected for the Galactic and internal reddening from the above literature. Finally, we also added two spectra of SN 2005ip on day 1, a few weeks after the SN explosion, and on day 93 after the discovery (Smith et al. 2009). Dust extinction to the SN component is treated as a free parameter with the extinction curve of $R_V = 3.1$ in Cardelli et al. (1989). Obvious narrow emission lines were masked during the fit.

For each SN template, we obtain the best-fitted parameters by minimizing χ^2. The least reduced χ^2 is then sorted out among these minima, and the corresponding SN template is considered as the best match. We find that SN 1999gi at day 1 provides the best fit (reduced chi-square χ^2_ν/dof $= 1.347/2803$), followed by SN 2006bp at day 1 ($\chi^2_\nu = 1.374/2865$), also a few days after the explosion. Other templates give a significantly worse fit due to a mismatch of bumps. As shown in Figure 1, these templates are still not able to sufficiently strongly reproduce the 4600 Å bump strength. Noticeably, there is a global deficit in the fit from

[8] http://supernova.lbl.gov/~nugent/nugent_templates.html
[9] http://suspect.nhn.ou.edu

Table 1
Narrow Emission Line Parameters[a]

Line	λ (Å)	σ[b] (km s^{-1})	Flux
[O II]λ3727	3727.30 ± 0.14	85 ± 8	39 ± 5
[O II]λ3729	3730.06	85	52 ± 5
[Ar XIV]λ4414	4414.28 ± 0.55	246 ± 22	39 ± 5
Hβ	4863.16 ± 0.15	122 ± 9	61 ± 4
[O III]λ4959	4960.91 ± 0.19	69[c]	4 ± 2
[O III]λ5007	5008.85	69	13 ± 3
[Fe XIV]λ5304	5304.34 ± 0.29	199 ± 17	80 ± 6
[Fe X]λ6376	6377.21 ± 0.34	251 ± 16	94 ± 6
[N II]λ6548	6550.29 ± 0.05	80 ± 2	21 ± 1
Hα	6565.10	80	152 ± 6
Hα	6566.40 ± 0.90	460 ± 59	99 ± 11
[N II]λ6583	6585.70	80	64 ± 3
[S II]λ6716	6718.80 ± 0.14	79 ± 6	35 ± 3
[S II]λ6731	6733.18	79	24 ± 3
[S XII]λ7612	7611.87 ± 0.90	142 ± 59	38 ± 11
[Fe XI]λ7894	7896.34 ± 0.37	145 ± 14	81 ± 7

Notes.
[a] Flux in units of 10^{-17} erg s^{-1} cm^{-2} in the observed frame.
[b] Including the SDSS instrument width of about 69 km s^{-1}.
[c] The value is pegged at the lower-limit during the fit.

the peak to the red side of the bump. The internal reddening of the SN is relatively small with $E(B-V) = 0.05$–0.10 for the SN199gi and SN2006bp templates. These templates give a consistent stellar velocity dispersion of $\sigma_* \simeq 30$ km s^{-1}. Because the value is well below the spectral resolution of SDSS and resolutions of IC templates and the SDSS spectrum are not perfectly matched, it can only be considered as an indication for a small stellar velocity dispersion. In passing, we note that the late spectrum of SN2005ip does not provide a fit to the SDSS spectrum, although the first day spectrum of SN2005ip gives a reasonable fit up to a wavelength of 4900 Å. Because the first day spectrum does not cover the wavelengths of the two blue bumps, which are the most prominent features in the spectrum of SDSS J0748+4712, it is not clear if SDSS J0748+4712 looks similar to SN2005ip at the early stage.

Because SN templates do not provide a good fit to the SDSS spectrum, we also considered another empirical model consisting of a blackbody and four Gaussians for bumps. With this description, we obtain a much better fit to the SDSS spectrum (χ^2_ν/dof = 1.159/3216; also Figure 1). The fit yields a temperature $(1.3 \pm 0.4) \times 10^4$ K and a moderate reddening $E(B-V) = 0.26 \pm 0.10$, marginally larger than the SN template fit. In the following, we will refer to this fit as our baseline model.

We measure narrow emission lines in the residual spectrum after subtraction of the model continuum. Each emission line is fitted with one Gaussian except for Hα, which requires an additional broad component. In the fit for [N II]λ6583 and Hα blending, the width and center of the two narrow components are locked in the velocity space. Continuum is modeled either as a local constant for isolated or close doublets, or as a linear function in [O III]+Hβ, Hα+[N II]+[S II] regimes. This scheme yields acceptable fits for all emission lines. The derived parameters are summarized in Table 1. Normal narrow lines, such as [O II]λ3727, [N II]λ6583, and Hα, have a width around $\sigma \simeq 40$ km s^{-1} after removal of the SDSS instrumental broadening of 69 km s^{-1}. Their redshifts are consistent with being the same. [O III]λ5007 is very weak. Hβ is somewhat broader, perhaps due to the inclusion of an intermediate component, which is prominent in Hα. The line ratios, [N II]λ6583/Hα and [O III]λ5007/Hβ are located in the H II regime on the BPT diagram (e.g., Kewley et al. 2006). Therefore, these normal narrow lines are likely dominated by H II regions of the galaxy. The Balmer decrement Hα/Hβ = 2.57 ± 0.21 is consistent with the Case-B recombination, indicating little dust extinction to the H II regions in the line with the low extinction of starlight inferred in the previous section. The [N II]λ6583/Hα and [S II]λ6716/Hα ratios suggest half a solar metallicity for the H II regions (Pettini & Pagel 2004). This is in line with the luminosity of galaxies ($M_r = -19.75$). The intermediate width component of Hα has a width of around 1500 km s^{-1} and a flux of 2/3 of the narrow component. Such a component may also be present in the Hβ line (Figure 3). As mentioned above, we did not include this component in the fit due to a low signal-to-noise ratio (S/N).

The coronal lines are much broader, but their profiles show subtle differences from one line to another (Figure 4). [Fe XI]λ7894 is the narrowest ($\sigma = 127 \pm 16$ km s^{-1}) and redshifted by ∼70 km s^{-1} with respect to Hα or [N II]. It is entirely possible that [Fe X]λ6376 has a profile similar to that of [Fe XI]λ7894. The core component of [Fe X]λ6376 is very similar to that of [Fe XI]λ7894, but there appears an additional weak blue component in [Fe X]λ6376 which may be due to the contamination of other lines. If this were verified, there would be a trend of higher ionization lines being blueshifted relative to lower ionization lines. Other high-ionization coronal lines are blueshifted by 40–130 km s^{-1} with respect to [Fe XI]λ7894. These differences are larger than the uncertainty of the SDSS spectral calibration. [Fe XIV]λ5304 profile is well defined and is broader (188 ± 18 km s^{-1}) than and blueshifted (-90 ± 21 km s^{-1}) with respect to [Fe XI]λ7894. [S XII]λ7612 is blueshifted (-130 ± 25 km s^{-1}), but with almost the same width (124 ± 24 km s^{-1}). [Ar XIV]λ4414 appears also blueshifted and broader, though with a low S/N. At a redshift of $z = 0.0616$, the line luminosities are (8.8, 7.4, 7.5, 3.6, and 3.5) × 10^{39} erg s^{-1}, for [Fe X]λ6376, [Fe XI]λ7894, [Fe XIV]λ5304, [S XII]λ7612, and [Ar XIV]λ4414 before correction for the internal reddening, which may affect the line luminosities by no more than 50%.

We also measure the narrow emission lines in the BAO spectra with a similar procedure, but without an SN continuum component. Despite the low S/N of either spectrum, the coronal lines are very weak if present at all (Figure 5). However, [O III]λ5007 is 10 times stronger than in the SDSS spectrum, suggesting the trend that low-ionization lines are being strengthened while high-ionization ones are being weakened (Figure 2).

3. THE EMISSION LINE REGION AND IONIZING CONTINUUM

3.1. The Coronal Line Emission Region

First we estimate the emission measure, $\mathrm{EM} = \int_V n_e n_{\rm ion} dV = \langle n_e n_{\rm ion} \rangle V$, or $\mathrm{EM} = n_e n_{\rm ion} V$ for a uniform medium of volume V, ion density $n_{\rm ion}$, and electron density n_e, assuming that collisional de-excitation and continuum fluorescence are unimportant. The observed line luminosity relates to EM with, e.g., $L(\mathrm{Fe\,X}) = C(T) n_e n(\mathrm{Fe}^{+9}) V = C(T) \mathrm{EM}_{\mathrm{Fe}^{+9}}$, where $C(T)$ is the collisional strength from the lower to the upper levels of the correspondent transition, which is a descending function of gas temperature T, and $n(\mathrm{Fe}^{+9})$ is the density of Fe^{+9}. If gas is photoionized, its temperature is around 10^5 K (e.g., Korista & Ferland 1989). We took the collisional excitation rates from the

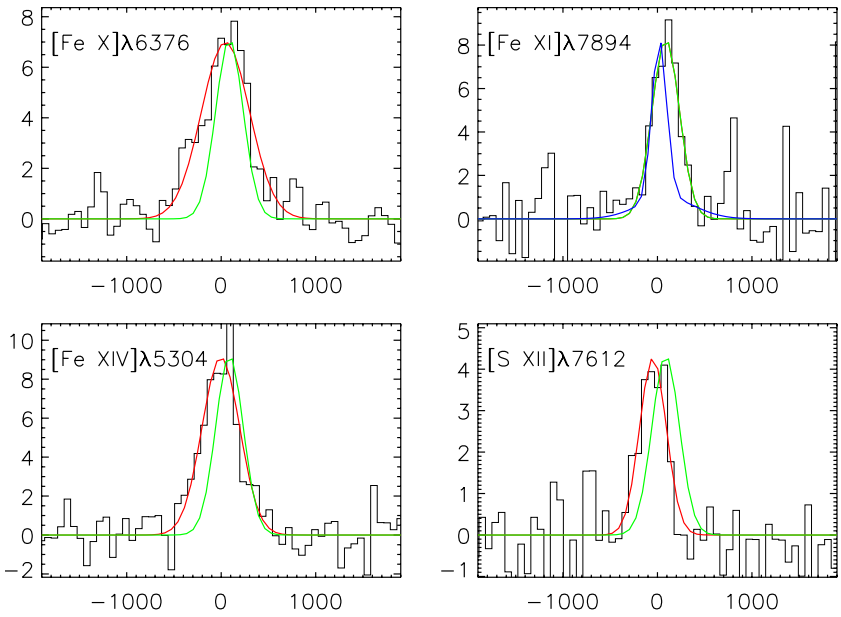

Figure 4. Observed profiles of coronal lines (in black) and their Gaussian models (in red). For comparison, the model profile of [Fe XI]λ7894 is overplotted in the green, while in the panel for [Fe XI]λ7894, the Hα line is shown in blue.

(A color version of this figure is available in the online journal.)

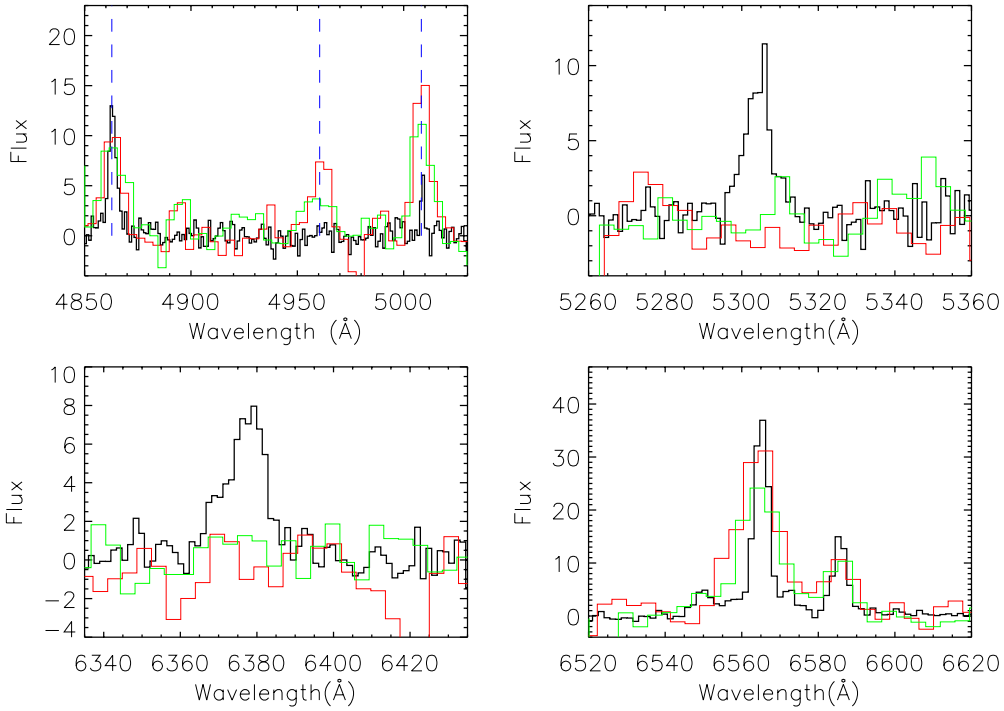

Figure 5. Variations of emission lines between SDSS (black) and BAO 2.16 m observations (red, green)—upper left: Hβ+[O III] lines; upper right: the [Fe XIV] line; lower left: [Fe X]; lower right: Hα+[N II].

(A color version of this figure is available in the online journal.)

atomic data archive of CHIANTI (Dere et al. 2009). This gives emission measures of 0.6, 2.5, 1.6, 1.9, and 1.2 $\times 10^{59}$ cm^{-3} for Fe^{+13}, Fe^{+10}, Fe^{+9}, S^{+11}, and Ar^{+13} using the observed line luminosities. Note that collisional ionized gas will have a much higher temperature (a few 10^6 K), thus a much lower $C(T)$, and requires one order of magnitude larger EM (Figure 6). Assuming a solar abundance for Ar, i.e., $n(\mathrm{Ar})/n(\mathrm{H}) = 2.51 \times 10^{-6}$, and Ar^{+13} being the dominant species of the atom, we can derive a minimum EM $\simeq n(\mathrm{H})^2 V \sim 5 \times 10^{64}$ [Ar/H]$^{-1}$ cm^{-3}. Other lines give the same order of magnitude, but a slightly lower EM. Considering an unknown ionization correction, they can be taken as all consistent. Since Ar, S, and Fe are synthesized only during SN explosions, it is unlikely that they are much more overabundant in the circumstellar medium unless the coronal line region (CLR) was polluted during the SN process, which seems less likely (see below).

Next, we explore what constraints on CLR can be imposed based on the above estimates. A minimum size of CLR can be

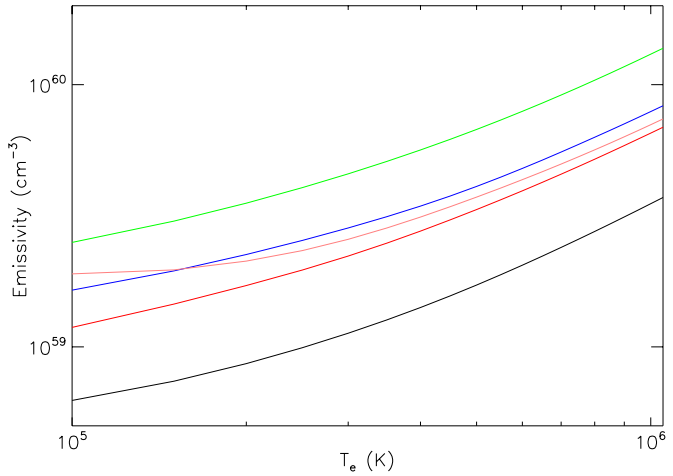

Figure 6. Emission measure ($n_e n_{\rm ion} V$, without internal extinction) as a function of gas temperature for Ar^{+13} (red), Fe^{+9} (blue), Fe^{+10} (green), Fe^{+13} (black), and S^{+11} (pink).

(A color version of this figure is available in the online journal.)

set in the first place. For a uniform, spherical CLR, the radius can be written as $R = 1.1\, n_9^{-2/3} {\rm EM}_{65}^{1/3} [{\rm Ar/H}]^{-1/3}$ lt days, where n_9 is the density in units of 10^9 cm^{-3}, and EM_{65} the emission measure in units of 10^{65} cm^{-3}. [Fe x] has the lowest critical density of 1.5×10^9 cm^{-3} among these detected coronal lines, and gas density should not be much larger than this. This gives a minimum size of CLR of one light day. On the other hand, with this minimum radius, the gaseous column density of CLR will be $N_{\rm H} = 3 \times 10^{24} {\rm EM}_{65}^{1/3} n_9^{1/3}$ [Ar/H]$^{-1/3}$ cm^{-2}. At this column density, CLR is optically thick to X-rays up to 10 keV. However, photoionization requires that CLR be optically thin to soft X-rays because these photons ionize the gas. To meet this constraint, CLR must be much larger than this minimum radius, i.e., having a much lower density. If the column density is less than a few 10^{23} cm^{-2}, CLR will be of order of a light year and the density around 10^6 cm^{-3}.

If gas in CLR is in a thin shell or clumpy, CLR can be smaller. In a thin shell case, the density and column density can be written as $n_{\rm H} = 7 \times 10^8 {\rm EM}_{65}^{1/3} \xi^{-1/2} R_{\rm lt\ day}^{-3/2}$ [Ar/H]$^{-1/2}$ cm^{-3} and $N_{\rm H} = 2 \times 10^{24} {\rm EM}_{65}^{1/3} \xi^{2/3} n_9^{1/3}$ [Ar/H]$^{-1/3}$ cm^{-2}, where $\xi = \Delta R/R$ is the relative thickness. For a given density and EM, a smaller ξ will result in a smaller column density and a larger radius. If $\xi = 10^{-3}$, the gaseous column density will be of order of a few 10^{22} cm^{-2}, which is still not very optically thick to soft X-rays, and CLR is of the order of 10 light days. The column density and density for clumpy gas should be in between the thin shell and the uniform sphere case. These exercises suggest that CLR should be larger than 10 light days in size.

Note in passing that, if collisional de-excitation is important, the above-estimated EM will only be a lower limit. On the other hand, Korista & Ferland (1989) showed that the far-UV (~300 Å) continuum pumping process accounts for nearly half of the coronal emission line intensity in Seyfert galaxies. The exact effect depends on the gas density and the shape of the ionizing continuum. For the minimum size estimated above, the density is around 10^9 cm^{-3}. At this density, collisions should dominate the excitation unless the far-UV radiation field is very strong. Thus, we believe that it will not affect the order of magnitude estimated above.

3.2. The Ionizing Source

We assume that gas is photoionized because collisional ionization will require much larger emissivity. The ionization potential of Fe^{+8}, Fe^{+9}, Fe^{+12}, S^{+10}, and Ar^{+12} are 233.6, 262.1, 361, 504, and 685.9 eV, so soft X-rays are required to ionize them. With the above estimated density, the recombination time of the gas is $1/(n_e \alpha(T))$, typically less than 1 hr for the ions listed above if $n_e > 10^8$ cm^{-3}. This should be shorter than the duration of X-ray radiation, while ionization is even shorter if these ions are the dominant species. Therefore, the gas is likely in a quasi-ionization equilibrium. In this case, we can estimate the ionizing photons absorbed by the corresponding ions from their coronal lines. Each ion stays at the upper level for an average time of $1/\alpha_{\rm eff}(T) n_e$ before it recombines to a lower ionization sate, where $\alpha_{\rm eff}$ is the recombination coefficient of excited states.[10] During that period, the ion is collisionally excited $n_e C(T)/\alpha_{\rm eff}(T) n_e$ times. If collisional de-excitation is not important, each collisional excitation will result in a coronal line photon. Thus, the absorbed ionization photon flux can be written as, taking [Fe x]λ6376 as an example,

$$\Phi({\rm Fe\ x}) \geqslant \frac{L({\rm Fe\ x})}{h\nu_{10}} \frac{\alpha_{\rm eff,Fe\ x}(T)}{C(T)}. \quad (1)$$

One can write similar equations for [Fe XI]λ7894, [Fe XIV]λ5304, [Ar XIV]λ4414, and [S XII]λ7612. By summing over all the terms on the left and right, we estimate that a minimal X-ray luminosity absorbed by these ions is ~50 of the total coronal line luminosity. Therefore, a minimum X-ray luminosity of a few 10^{42} erg s^{-1} is required to power the coronal lines in a photoionization equilibrium model. This estimate is in-exact because we have not considered two important processes. First, recombination to lower levels will emit a photon that may be able to ionize other ions. The re-emitted photons are distributed nearly isotropic with an average delay of recombination time with respect to the incident ionizing radiation. Second, the ionization of other ions requires additional X-rays. For example, when [Fe x]λ6376 to [Fe XIV]λ5304 become dominant species, hydrogen and helium-like oxygen, lithium-like neon, magnesium, and L-shell silicon are by a factor of 10 more abundant than Fe^{+10}, Fe^{+11}, Fe^{+14}, S^{+12}, and Ar^{+14} for a gas with solar metallicity. Giving that the two effects are opposite, we believe that it still gives a reasonable order of magnitude estimate. Note that the above-estimated X-ray luminosity is much lower than the X-ray luminosity of Seyfert galaxies with a similar coronal line luminosity ($\log(f_{\rm [Fe\ XI]}/f_X) = (-3.52 \pm 0.38)$ and $\log(f_{\rm [Fe\ X]}/f_X) = (-3.43 \pm 0.55)$; Gelbord et al. 2009).

As discussed in Section 3.1, it is quite possible that a coronal line emission sustains for years, although we only have an upper limit of four years to the decay time. In this case, the total energy in coronal lines would be about a few ~10^{47} erg. According to the above estimate, this requires a total energy in soft X-rays of 10^{49} erg to power CLR. In addition, a large number of UV photons is required to ionize light elements, such as hydrogen, helium, etc. It should be noted that coronal lines can be ionized by an active X-ray source or they may be echoes of a past soft X-ray flare on an extended medium.

[10] Recombination to the ground state will give rise to an ionizing photon.

4. THE NATURE OF SUPERSTRONG CORONAL LINE EMITTERS

4.1. A Class of Superstrong Coronal Emission Galaxies?

SDSS J0748+4712 is the second SSCLE reported to show large line variations on a timescale of years. It shares many common properties with the first such object, SDSS J0952+2143 (Komossa et al. 2008, 2009). Coronal lines are among the strongest narrow lines. [Fe X]λ6376 is as strong as [O III]λ5007 in SDSS J0952+2143, and all high-ionization coronal lines are several times stronger than [O III]λ5007 in SDSS J0748+4712. An intermediate-width component of Balmer lines is present in the SDSS spectra of both objects, although it is much stronger in SDSS J0952+2143. In either object, high-ionization coronal lines fade while low-ionization lines remain constant or even increase years after its discovery. In SDSS J0952+2143, high-ionization lines [Fe XIV]λ5304, [Fe XI]λ7894, and [Fe X]λ6376 decreased by a factor of 10 from 2005 to 2008, while [Fe VII]λ6087 by only 30% and [O III]λ5007 even slightly increased; in SDSS J0748+4712, coronal lines disappeared while [O III] increased by a factor of 10 from 2004 to 2009. But there are some obvious differences in their SDSS discovery spectra. The SDSS spectrum of SDSS J0748+4712 displays prominent broad bumps and high-ionization coronal lines but no [Fe VII] and He II λ4686, while the spectrum of the latter does not show such bumps but prominent [Fe VII] and He II. Also, intermediate width Balmer lines are much weaker in SDSS J0748+4712 than in SDSS J0952+2143. Note that [Fe X]λ6376 luminosity in SDSS J0748+4712 is five times lower than in SDSS J0952+2143. We found four more SSCLEs in the SDSS spectroscopic sample of galaxies (including the one in Gelbord et al. 2009): two without [Fe VII] emission while another two similar to SDSS J0952+2143.

The similarity between SSCLEs with and without [Fe VII]λ6087 indicates that they are the same type of object, while decreasing ionization over time in both objects suggests that different ionization of the line spectrum observed may be unified in a time evolution picture. SDSS J0748+4712 was observed earliest among them, so it shows the highest ionization level and also displays continuum and bump emission. As time passed, the broad bumps disappeared and intermediate width Balmer lines increased, and the ionization of CLR decreased. Later on, both [Fe XIV],[Fe X] and intermediate width Balmer lines weakened, while [O III] and [Fe VII] strengthen. Further on, both coronal lines and the intermediate width component of Balmer lines disappeared, and [O III] and low-ionization narrow lines further brightened. The timescale for such evolution is three to five years. Future, continuous monitoring of objects similar to SDSS J0748+4712 can verify this picture.

4.2. A Type II Supernova?

Three pieces of evidence point to an SN-like activity in SDSS J0748+4712: 0.1–0.2 magnitude brightening between the SDSS spectroscopic and photometric observations; three broad bumps in the SDSS spectrum similar to those seen in the spectra of some young SNe; and the vanishing of such features and coronal lines in the spectra taken four years later. By comparing SDSS photometric data with the SDSS spectrum, we estimated absolute magnitudes of the SN-like flare with −16.7, −16.7, and −17.4 at g, r, and i bands before correction for internal extinctions. The internal reddening correcting was quite modest (<0.4 mag in g). This places its optical luminosity well in the range of a Type II-P supernova (Poznanski et al. 2009).

The broad bumps are similar to those in the spectra of Type II-P SNe a few days after the shock breakout. In Type II-P SN 2006bp, Dessart et al. (2008) identified the bump around 4000 Å as blended emission lines N III λλ4001–4099, around 4600 Å as a blend of He II λ4686, N III λ4638, C III λ4647, and H I λ4861, and around 6500 Å a mixture of H I and He I. With this interpretation, the stronger 4600 Å bump and weak or absent He I 5760 Å bump, in comparison with SN 2005ip, indicate stronger He II emission, thus a higher photosphere temperature. Notice that the 4600 Å bump evolved very fast in the first few days due to a rapid decrease of the photosphere temperature (Dessart et al. 2008), and SN 1999gi, SN 2006bp are the only Type II-P known today to have been observed so early in the optical spectra showing He II emission lines. It is unclear whether a spectrum taken at a slightly earlier time than the above two SNe will show a 4600 Å bump as strong as the one observed in this object, and whether other type core-collapse SNe at the early phase can also reproduce a similar spectral feature. An intermediate width Hα line is seen in the residual spectrum. Such a line is usually considered as to arise from an interaction of the SN with its circumstellar medium (CSM; Filippenko 1997; Pastorello et al. 2002; Smith et al. 2010). The presence of such material can be considered as evidence for a massive SN progenitor, which tends to support a core-collapse SN.

Even though a young SN II-P is a plausible explanation for the photometric variation and the broad bumps seen in the SDSS spectrum, such a scenario has several drawbacks in explaining coronal line emission. First, the X-ray from a young Type II-P SN is insufficient to power the coronal lines. As noted in the last section, the total amount of energy in the soft X-rays is likely greater than 10^{49} erg s^{-1}. If this energy is released in the shock breakout, which lasts for about 10^3 s, then the X-ray luminosity would be 10^{46} erg s^{-1}. This is several orders of magnitude higher than expected of X-ray emission from a Type II SN (e.g., Soderberg et al. 2008; Nakar & Sari 2010). Alternatively, the ionizing X-rays are produced in the shock of a blast wave into the dense CSM. However, according to Chevalier & Fransson (1994), interaction of the expanding shell with the CSM can produce an X-ray luminosity of $2.4\times10^{41}\mathrm{EM}_{65}^{2/3}n_9^{1/3}v_{s4}^3$ erg s^{-1}, assuming half of the X-rays are absorbed by the shell, where v_{s4} is the shock velocity in units of 10^4 km s^{-1} and n_9 is the particle density at the shock frontier in units of 10^9 cm^{-3} for a uniform spherical wind. This X-ray luminosity is an order of magnitude lower than that required to power the coronal lines if reasonable parameters are used. This energy budget has already been noted by Komossa et al. (2009).

Second, the SN template fit suggests that the SN is very young, only a few days old after the shock breakout. If the coronal line emission is related to SNe, the observed time of the CLR at SDSS should be less than the light travel distance of the age of the SN.[11] However, a CLR of at least 10 light days is required to account for the high coronal line luminosity as discussed in Section 3.2.

Finally, the width of the coronal lines is not consistent with an RSG progenitor of the Type II-P SN. Because the line width

[11] In the case of a continuum flare during the SN breakout, the intense UV/X-ray ionizing photons will ionize the surrounding CSM as they travel. The ionized bubble expands nearly at the speed of light from the optically thin region to the ionizing continuum for the ionization parameters concerned here, but stalled after that. Due to the light traveling effect, the observed line photons come from a thick shell around the parabolic iso-delay surface, with a lag of SN age and a width of continuum duration, that intersects the CSM, in the optically thin case. In the case of $n(r)\propto r^{-2}$, taking into account such a delay will give a correction of order unity.

is 300–450 km s^{-1} in the FWHM, it cannot be formed in the shock region itself, which has a much larger velocity, or the post-shock region because the expanding shell is opaque to these lines. Rather, it must be emitted from the pre-shocked region, as in the case of SN 2005ip (Smith et al. 2009). Also our analysis in Section 3.2 shows that the CLR is much larger than the expanding shell. Thus, the kinematics of coronal line emitting gas reflects the undisturbed CSM. In this case, the line is broadened due to the differently projected velocity of wind, which must be a few hundred km s^{-1}. This requires a compact progenitor rather than an RSG, which produces a wind of 15 km s^{-1}. In view of these problems, if the SN is responsible for the strong coronal line emission, it must be very different from any known SN.

4.3. Tidal Disruption

Tidal disruption of a star by a supermassive/intermediate mass black hole produces a flare, fading on timescales from several months to a year, in UV and X-rays with a peak luminosity close to an Eddington one, once some of the debris falls back to form an accretion disk around the black hole (e.g., Rees 1988). A systematic search in the X-ray, UV, and optical has led to the discovery of a dozen candidates (Komossa & Bade 1999; Halpern et al. 2004; Esquej et al. 2008; Rosswog et al. 2009; Maksym et al. 2010; Gezari et al. 2009). Komossa et al. (2008) proposed that tidal disruption may also be responsible for variable coronal line emission. Both the SDSS and our spectrum include the galactic center, which should be considered as well. Komossa et al. (2009) pointed out that tidal disruption can potentially account for the observed emission line and continuum properties of SDSS J0952+2143, although a detailed model prediction is still lacking. UV and X-ray radiation from the accretion disk is a natural ionizing source. When the flare illuminates surrounding gas, it ionizes and excites gas giving rise to broad and narrow emission lines depending on the gas kinematics. The variable intermediate-width double horn Balmer lines in that object were interpreted as coming from unbounded tidal debris illuminated by the central radiation, while coronal lines are formed by the dense circumnuclear gas.

Much of their arguments are valid for SDSS J0748+4712 as well. When the central back hole is greater than $10^5\ M_\odot$, the accretion disk can account for high, soft X-ray ionizing photons. A black hole of 10^5–$10^6\ M_\odot$ in the galactic center is entirely possible given the luminosity of the galaxy ($M_K = -22.2$), although much larger than this can be ruled out from stellar velocity dispersion measurement (Tremaine et al. 2002). If CLR is virialized and dominated by the gravity of the black hole, gas at $10^6 r_g$ will produce a line width around 300–400 km s^{-1} (FWHM), similar to the observed coronal line width. A black hole with a mass of 10^5–$10^6\ M_\odot$ corresponds to the size of a few 10 light days, which meet the constraints in Section 3.2.

Photometric variations and broad bumps in the spectrum can put additional constraints on the tidal disruption model. The accretion rate, or luminosity, is determined by the fall-back rate of bounded tidal debris, which decreases with time as $t^{-5/3}$ after reaching its peak (Rees 1988; c.f. Lodato et al. 2009). The target was brighter during the SDSS spectroscopic observation than during the photometric observation. This set an upper limit to the age of disruption event to 4 months during the SDSS spectroscopic observation of SDSS J0748+4712. The flare has an absolute optical magnitude of $M_g = -17.3$ during the spectroscopic observation, which is on the same order of magnitude as predicted by some models for a $10^6\ M_\odot$ black hole (e.g., Strubbe & Quataert 2009).

The broad bumps probably can be interpreted as optical emission lines. Strubbe & Quataert (2009) argued that most tidal debris should blow away at an early point, leaving very broad optical emission lines in the spectrum for 10^5–$10^6\ M_\odot$ black holes. In their model, the strongest lines are Balmers, which cannot explain strong bumps in the SDSS spectrum of SDSS J0748+4712. However, if a star has evolved strongly, much of its hydrogen envelope has been stripped off. Tidal debris should then be helium-enriched, which may explain the strong blueshifted He II line. It should be noted that the bumps around 4600 Å can be fairly well fitted with a combination of He II, Hβ, and 6560 Å with Hα, with their line centers and widths locked. A detailed physical model, which is beyond the scope of this paper, is certainly needed to verify this explanation.

5. CONCLUSION

We detected broad bumps reminiscent of a young Type II-P supernova and strong high-ionization coronal lines in the spectrum of SDSS J0748+4712. The coronal line luminosity is typical of Seyfert galaxies, but other narrow lines suggest a normal star-forming galaxy. The source brightened by about 0.2 mag in the g band from the SDSS imaging to the SDSS spectroscopic observations over 4 months. These bumps and coronal lines disappeared in the spectra taken four to five years later, while the [O III] line increased by a factor of 10. The variation trend is similar to another SSCLE reported previously, suggesting the same physical origin. The different properties of the two objects may be ascribed to different observed evolution stages.

We set a robust lower limit on the size of CLR to be 10 light days and on the total energy of the ionizing continuum in soft X-rays to be 10^{49} erg. The size of the emission line region, high soft X-ray luminosity, and broad width of coronal lines cannot be understood in the young Type II-P supernova context. If coronal lines are indeed associated with an SN explosion, then the SN must be very different from that currently known. We argued that tidal disruption of the evolved star by a massive black hole may provide a viable explanation for the bumps and coronal lines. In this model, the bumps are considered as broad emission lines from winds produced during the tidal disruption process (Strubbe & Quataert 2009) of the partially evolved star.

A critical test to the above scenario should come from continuous monitoring of the spectral evolution and early follow-up of other bands, such as X-ray, UV, and infrared, shortly after the discovery of the coronal line emitter. X-ray and UV emission from a SN, predicted in the current model, drops very fast after a few hours and up to 10 days (Nakar & Sari 2010), while in the tidal disruption model, the tidal debris is accreted on the timescale of years (e.g., Lodato et al. 2009). We found that the absolute magnitude of the flare in the *GALEX* NUV band was −17.3 at 20 days after the SDSS spectroscopic observation for SDSS J0748+4712, which is brighter than what was predicted by SN models, but consistent with the tidal disruption model. We plan to carry out such a survey with the future Chinese spectroscopic survey telescope—LAMOST and conduct early follow-up observations of such events with other observatories.

We are grateful to the referees for their thorough reading and critical comments that led to a significantly improved paper, and to Dr. Nathan Smith for providing the spectra of SN 2005ip.

This work was supported by the Chinese NSF through NSF-10973013, 10973012, and 11033007, the national 973 program 2007CB815403 and 05, and CAS knowledge innovation project No. 1730812341. D.X. acknowledges support from the Chinese NSF under grant NSFC 10873017, and from program 973 (2009CB824800). This work has made use of the data obtained by SDSS and by the 2.16 m optical telescope on Xinglong Station, Chinese National observatories. Funding for the SDSS and SDSS-II has been provided by the Alfred P. Sloan Foundation, the Participating Institutions, the National Science Foundation, the U.S. Department of Energy, the National Aeronautics and Space Administration, the Japanese Monbukagakusho, the Max Planck Society, and the Higher Education Funding Council for England. The SDSS Web site is http://www.sdss.org/.

REFERENCES

Adelman-McCarthy, J. K., Agüeros, M. A., Allam, S. S., et al. 2008, ApJS, 175, 297
Bade, N., Komossa, S., & Dahlem, M. 1996, A&A, 309, L35
Cardelli, J. A., Clayton, G. C., & Mathis, J. S. 1989, ApJ, 345, 245
Chevalier, R. A., & Fransson, C. 1994, ApJ, 420, 268
Dere, K. P., Landi, E., Young, P. R., et al. 2009, A&A, 498, 915
Dessart, L., Blondin, S., Brown, P. J., et al. 2008, ApJ, 675, 644
Esquej, P., Saxton, R. D., Komossa, S., et al. 2008, A&A, 489, 543
Filippenko, A. V. 1997, ARA&A, 35, 309
Filippenko, A. V., & Korth, S. 1991, IAU Circ., 5234, 1
Gelbord, J. M., Mullaney, J. R., & Ward, M. J. 2009, MNRAS, 397, 172
Gezari, S., Heckman, T., Cenko, S. B., et al. 2009, ApJ, 698, 1367
Gröningsson, P., Fransson, C., Lundqvist, P., et al. 2006, A&A, 456, 581
Halpern, J. P., Gezari, S., & Komossa, S. 2004, ApJ, 604, 572
Immler, S., Brown, P. J., Milne, P., et al. 2007, ApJ, 664, 435
Kewley, L. J., Groves, B., Kauffmann, G., & Heckman, T. 2006, MNRAS, 372, 961
Komossa, S., & Bade, N. 1999, A&A, 343, 775
Komossa, S., Halpern, J., Schartel, N., et al. 2004, ApJ, 603, L17
Komossa, S., Zhou, H., Rau, A., et al. 2009, ApJ, 701, 105
Komossa, S., Zhou, H., Wang, T., et al. 2008, ApJ, 678, L13
Korista, K. T., & Ferland, G. J. 1989, ApJ, 343, 678
Leonard, D. C., Filippenko, A. V., Li, W., et al. 2002, AJ, 124, 2490
Lodato, G., King, A. R., & Pringle, J. E. 2009, MNRAS, 392, 332
Lu, H., Zhou, H., Wang, J., et al. 2006, AJ, 131, 790
Maksym, W. P., Ulmer, M. P., & Eracleous, M. 2010, ApJ, 722, 1035
Matheson, T., Filippenko, A. V., Li, W., Leonard, D. C., & Shields, J. C. 2001, AJ, 121, 1648
Nakar, E., & Sari, R. 2010, ApJ, 725, 904
Pastorello, A., Turatto, M., Benetti, S., et al. 2002, MNRAS, 333, 27
Pettini, M., & Pagel, B. E. J. 2004, MNRAS, 348, L59
Poznanski, D., Butler, N., Filippenko, A. V., et al. 2009, ApJ, 694, 1067
Quimby, R. M., Wheeler, J. C., Höflich, P., et al. 2007, ApJ, 666, 1093
Rees, M. J. 1988, Nature, 333, 523
Rosswog, S., Ramirez-Ruiz, E., & Hix, W. R. 2009, ApJ, 695, 404
Schlegel, D. J., Finkbeiner, D. P., & Davis, M. 1998, ApJ, 500, 525
Smith, N., Chornock, R., Silverman, J. M., Filippenko, A. V., & Foley, R. J. 2010, ApJ, 709, 856
Smith, N., Silverman, J. M., Chornock, R., et al. 2009, ApJ, 695, 1334
Soderberg, A. M., Berger, E., Page, K. L., et al. 2008, Nature, 453, 469
Strubbe, L., & Quataert, E. 2009, MNRAS, 400, 2070
Tremaine, S., Gebhardt, K., Bender, R., et al. 2002, ApJ, 574, 740
York, D. G., Adelman, J., Anderson, J. E., Jr., et al. 2000, AJ, 120, 1579